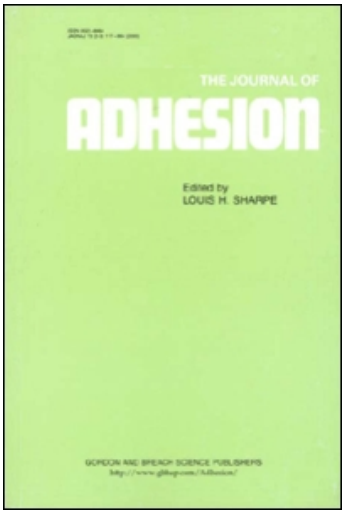

The Journal of Adhesion
Publication details, including instructions for authors and subscription information:
http://www.informaworld.com/smpp/title~content=t713453635

Mechanical Detachment of Nanometer Particles Strongly Adhering to a Substrate: An Application of Corrosive Tribology

J. T. Dickinson[a]; R. F. Hariadi[a]; S. C. Langford[a]
[a] Department of Physics and Materials Science Program, Washington State University, Pullman, WA, USA

To cite this Article Dickinson, J. T. , Hariadi, R. F. and Langford, S. C.(2000) 'Mechanical Detachment of Nanometer Particles Strongly Adhering to a Substrate: An Application of Corrosive Tribology', The Journal of Adhesion, 74: 1, 373 — 390
To link to this Article: DOI: 10.1080/00218460008034537
URL: http://dx.doi.org/10.1080/00218460008034537

J. Adhesion, 2000, Vol. 74, pp. 373–390
Reprints available directly from the publisher
Photocopying permitted by license only

Mechanical Detachment of Nanometer Particles Strongly Adhering to a Substrate: An Application of Corrosive Tribology

J. T. DICKINSON*, R. F. HARIADI and S. C. LANGFORD

Department of Physics and Materials Science Program, Washington State University, Pullman, WA 99164-2814, USA

(Received 25 June 1999; In final form 14 October 1999)

The tip of a scanning probe microscope was used to detach nanometer-scale, single crystal NaCl particles grown on soda lime glass substrates. After imaging a particle at low contact forces, a single line scan at high contact force was used to detach the particle from the substrate. The peak lateral force at detachment is a strong function of particle contact area and humidity. As the relative humidity is raised from low to high values, the strength of the particle-substrate bond decreases dramatically. We interpret these results in terms of detachment by chemically-assisted crack growth along the NaCl-glass interface. Numerical estimates of the electrostatic and dispersive contributions to the work of adhesion are also discussed.

Keywords: Particle removal; Humidity effects; Scanning force microscopy; Crack growth, chemically assisted; Work of adhesion, Model

1. INTRODUCTION

Particles smaller than about a micron in diameter can be extremely difficult to remove from many surfaces. The technologies of chemical-mechanical polishing [1] and laser-assisted particle removal [2, 3], among others, have been developed in part to ensure that such

*Corresponding author. Tel.: (509) 335-4914, Fax: (509) 335-7816, e-mail: jtd@wsu.edu

particles are removed prior to critical surface operations. Particle removal is often facilitated by the presence of a liquid phase, which reduces the adhesive forces binding the particle to the substrate. The nature of the interfacial binding forces, the character and role of interfacial defects, and the effect of the liquid phase are not presently well understood.

In this work, we study the effect of humidity on the force required to detach submicron salt crystals from soda lime glass substrates. The chemical activity of water vapor is readily varied over a wide range by changing the pressure of the vapor. Particles were detached with the tip of a scanning force microscope (SFM). The SFM tip is analogous to a well-characterized asperity which "rubs" adhering particles from the substrate. Sodium chloride crystals of the appropriate size are readily grown by evaporation from a dilute aqueous NaCl solution. The resulting crystals adhere strongly to soda lime glass, forming symmetric protrusions on a reasonably flat substrate. Both NaCl and soda lime glass are hydrophilic and, thus, interact strongly with water. The effect of water vapor on crack growth in soda lime glass has been well studied [2].

Previous studies of particle adhesion using scanning probe microscopy include that of Meyer *et al.* [3] (adhesion and motion of C_{60} molecules on NaCl) and Junno *et al.* [4] (silver particles on semiconductor surfaces). Lebreton *et al.* [5] found that atom removal with scanning tunneling microscopy (STM) was facilitated by humidities above a critical value. Significantly, a large fraction of the interfacial bonds binding very small particles to the substrate lie along their perimeter; this strongly amplifies the response of the particle to chemically active agents in the surrounding atmosphere. In this work, we show that raising the humidity from low values dramatically lowers the lateral force required to fracture the NaCl-glass bond as the SFM tip is drawn across the particle.

2. EXPERIMENT

Submicron NaCl crystals were deposited on soda lime glass substrates by dissolving 1 – 3 grains ($\sim 1\,mm^3$) of commercial salt in a drop of de-ionized water on a clean microscope glass slide. The solution

was gently spread across the slide with a cotton swab and allowed to evaporate to dryness at room humidity and temperature. Both evaporation and sample storage were under ambient laboratory atmosphere conditions – typically 20 – 40% relative humidity (RH).

A Digital Instruments (Santa Barbara, CA) Nanoscope III scanning force microscope mounted in a controlled environment chamber was used to image and manipulate the particles. This work employed commercial Digital Instruments Si_3N_4 cantilevers. A representative sample of tips was characterized by imaging niobium "artifacts" from Electron Microscopy Sciences, Fort Washington, PA [6], yielding an average tip radius of 37 ± 4 nm. This value is consistent with previous measurements in our laboratory, as well as radii measurements inferred from image deconvolution. Due to the small size of the NaCl crystals employed in this work, deconvolution significantly improved our measurements of particle dimensions. Deconvolution was performed with the DECONVO program from Silicon-MDT of Moscow, Russia [7, 8]. As the particle bases are not imaged, even in the deconvoluted images, the area of the top of the particle was taken as the particle area. This is equivalent to assuming that the particles are rectangular parallelepipeds, like their macroscopic counterparts in table salt.

Considerable effort was devoted to tip characterization and calibration. The spring constant for normal deflections, k_{normal}, of a sample of typical SFM cantilevers was determined by analyzing the power spectra of thermal fluctuations in the cantilever deflection [9 – 11], yielding $k_{normal} = 0.31$ N/m. The spring constant for lateral deflections, $k_{lateral}$, was estimated by multiplying k_{normal} by the expected $k_{normal} : k_{lateral}$ (0.0032, from finite element calculations [12]), yielding $k_{lateral} = 96$ N/m [13]. This k_{normal} to $k_{lateral}$ ratio is within 5% of an experimental measurement using the method outlined by Bhushan *et al.* [14]. The detector sensitivity in the normal direction was determined to be 9.22 nm/V by performing the force calibration procedure on a stiff substrate (aluminum oxide), where the deformation of the substrate and tip can be neglected [3].

Particle detachment experiments were initiated by setting the humidity to the desired value by adjusting the flow of dry air and humidified air into the chamber. The RH in the chamber was continuously measured with a BioForce Laboratory humidity sensor.

The glass surface was then scanned in contact mode to locate attached particles of the appropriate size. High tip velocities (typically 42 μm/s) and low applied normal forces (less than 20 nN) were employed during imaging to minimize the effect of scanning on particle adhesion. Scanning was continued until the tip was positioned to cross the center of the chosen particle (the white line in Fig. 1(b)); then the contact force raised to a high value (≤ 320 nN).

When an appropriate particle was found, the tip was positioned to cross the center of the chosen particle and the tip speed reduced to 0.20 μm/s. As the tip approached the particle, the normal force was raised to a high value (180 – 320 nN). Given a particle of the appropriate size, the particle would then be detached from the substrate upon the tip's first encounter with the particle. After each detachment event, the signal corresponding to zero lateral force was determined by averaging the signals during trace and retrace portions of the linear scan.

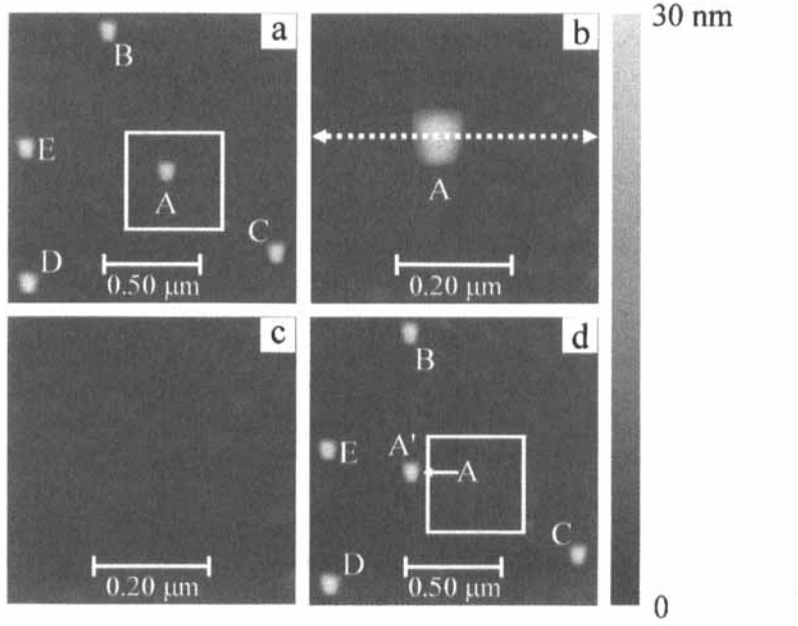

FIGURE 1 Low contact force images of NaCl particles (a) before particle removal, (b) a close-up immediately prior to the linear scan that removed the particle, (c) a close-up immediately after the line scan that removed the particle, and (d) an additional scan of region imaged in (a), showing the removed particle at the end of the 500 nm linear scan.

Subsequently, low contact force, high scan rate images were acquired to locate the detached particle. Room temperature during data acquisition was typically between 21 and 24°C.

3. RESULTS

Images taken before and after particle detachment at low RH are shown in Figure 1. Particle A in Figure 1(a) was selected for removal, and imaged at higher magnification in Figure 1(b). Note that the rectangular form of the particles in these images reflects the pyramidal tip geometry and not the actual particle shape. After aligning the SFM along the dotted line in Figure 1(b), the contact force was raised to a high value and the tip was drawn once across the position of the particle. Low contact force imaging was then resumed, confirming that the particle had indeed been removed (Fig. 1(c)). Imaging at lower magnification (Fig. 1(d)) subsequently located the detached particle at the end of the high contact force scan. Subsequent images do not always show the detached particle, especially at high relative humidities. Although it is possible that these particles are forcibly ejected some distance after detachment (a "slap shot"), it appears that these particles often adhere to the SFM tip and are moved some distance without being imaged.

Typical height and lateral force signals during scanning across a NaCl particle at 10% RH are shown in Figure 2. The signals in Figures 2(a) and 2(c) were acquired at low applied normal forces (10 nN) and high tip velocities (42 μm/s) prior to particle detachment. The height signal in Figure 2(a) shows the particle profile, while the lateral force signal in Figure 2(c) shows characteristic upward and downward spikes as the tip slides up onto and down off of the sample, respectively. Interestingly, the lateral force as the tip passes over the center of the NaCl particle is measurably lower than the lateral force as the tip passes over the glass substrate. This difference cannot be attributed to elastic deformation effects, as the glass is actually stiffer than the NaCl. Young's modulus in soda lime glass is typically about 73 GPa; in NaCl the modulus (directionally averaged) is 37 GPa [15]. The salt-to-glass lateral force ratio ranges from about 0.8 at 3% RH to 0.3 at 68% RH. The changes in lateral force with humidity suggest

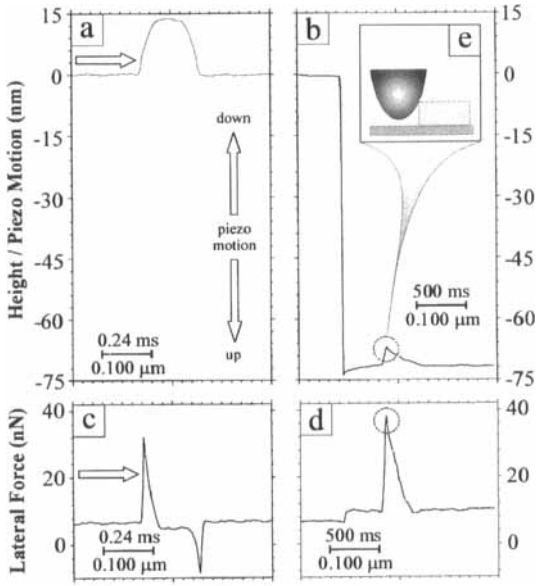

FIGURE 2 (a) and (b) Height, (c) and (d) lateral force signals during the low contact force scan used to align the tip on the particle, and during the slow, high contact force scan used to remove the particle from the substrate. Inset (e) shows the tip and NaCl position just before fracture.

that the adsorbed water layer on these hydrophilic surfaces strongly affects the apparent coefficient of friction, perhaps due to capillary effects.

The height and lateral force signals during detachment are shown in Figures 2(b) and 2(d). The tip velocity was reduced from 42 μm/s to 0.20 μm/s before beginning this scan. Approximately a quarter of the way through the scan, the nominal contact force was raised to 57 nN, producing a dramatic drop in the height signal of Figure 2(b). (To increase the normal force, the piezoelectric transducer must move downward, which changes the height signal in much the same way as a change in topography.) Increasing the normal force also produced a small, stepwise increase in the lateral force signal (Fig. 2(d)) due to the accompanying increase in friction. Midway through the scan, the tip encountered the particle, lifting slightly ($\sim$4 nm) onto the edge of the particle before detachment. Because the tip is not in contact with the glass at the moment of detachment (Fig. 2(b)), the friction between the tip and the glass does not contribute

to the measured lateral force at detachment. Thus, the entire lateral force at detachment is applied to the particle, and it is this force that induces detachment.

We identify the peak in lateral force and height signals with the detachment event itself. An upper bound on the energy per unit area required to fracture the interface is provided by the area under the rising portion of the lateral force *vs.* displacement plot prior to failure. In Figure 2(d), this amounts to about $50\,mJ/m^2$. In the fracture of more-macroscopic, highly-brittle samples (including soda lime glass and NaCl), it is not uncommon for two-thirds of this energy to be dissipated *via* plastic deformation and similar processes. Since plastic deformation is strongly hindered in nanometer-scale systems [16], its role in the removal of nanometer-scale particles is an open question.

Both the height and lateral force signals show distinct tails after detachment. Their duration depends strongly on RH and can extend much further than the physical extent of the particle. Thus, these tails cannot be attributed to incomplete detachment. We attribute these tails to the gradual drop in lateral force as the particle slips out from under the SFM tip. At low RH, the particle slides more freely along the glass, and the lateral force drops rapidly. However, at high RH, the particle encounters wet glass and slides more slowly.

The peak lateral force (at detachment) is a strong function of tip velocity. Figure 3 displays the lateral force signal during two successive

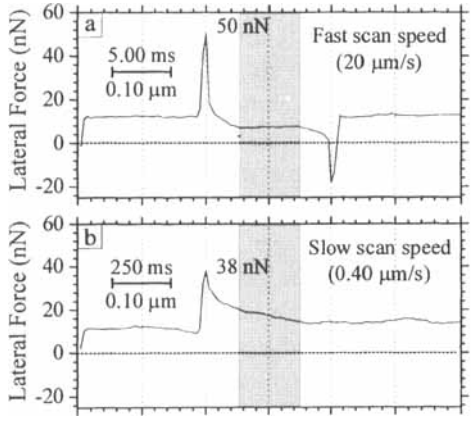

FIGURE 3 Lateral force signal during linear scans across the same NaCl particle at tip velocities of (a) 20 μm/s and (b) 0.40 μm/s. The normal force in each case was 17 nN.

linear scans across the same NaCl particle at an applied normal force of 17 nN and a high relative humidity (51%). After the scan of Figure 3(a) and before the scan of Figure 3(b), the tip velocity was reduced from 20 μm/s to 0.40 μm/s. During the first scan (at 20 μm/s), the SFM tip passes cleanly over the particle. However, during the slow scan (at 0.4 μm/s) the particle is detached. Furthermore, the peak lateral force during the slow scan (38 nN) is significantly lower than the peak lateral force during the fast scan (50 nN), which did not remove the particle. Experience indicates that a single scan at the faster rate of 20 μm/s does not significantly weaken the NaCl/glass bond. (A large number of scans at 20 μm/s do weaken the interface.) The dramatic effect of scan rate suggests that the duration of the applied force is critical, and that particle detachment is not merely due to the application of some critical stress associated with the intrinsic strength of the interface.

These results suggest that particle detachment involves the relatively slow growth of an interfacial crack. At low scan rates, relatively low crack velocities can detach the particle before the SFM tip passes onto the particle. Lower stresses are required to produce these lower crack velocities, so that failure occurs at lower applied lateral forces. At high scan rates, particle detachment during tip-particle contact requires higher crack velocities and higher lateral forces. The failure stresses reported below were all determined with a minimum of prior, low contact force scanning at relatively high tip velocities (>42 μm/s) and low contact forces (<20 nN), followed by a single, high contact force scan (typically 150 nN) at tip velocity of 0.20 μm/s. This procedure yielded consistent failure stress measurements. The crack velocities required for particle detachment at these scan rates (1 – 10 μm/s) are very low – consistent with crack velocities measured in soda lime glass and similar materials at low stresses in chemically-active environments [2].

For comparison purposes, we define a nominal shear strength, σ_c, of the interface equal to the peak lateral force divided by interfacial area, A. Values of σ_c from a large number of particle detachment events at several relative humidities are plotted in Figure 4 as a function of particle size. We have scaled the values of σ_c for 3% RH by a factor of ten for presentation purposes; the smallest particle at 3% RH failed at an nominal shear stress of 55 MPa. At lower humidities,

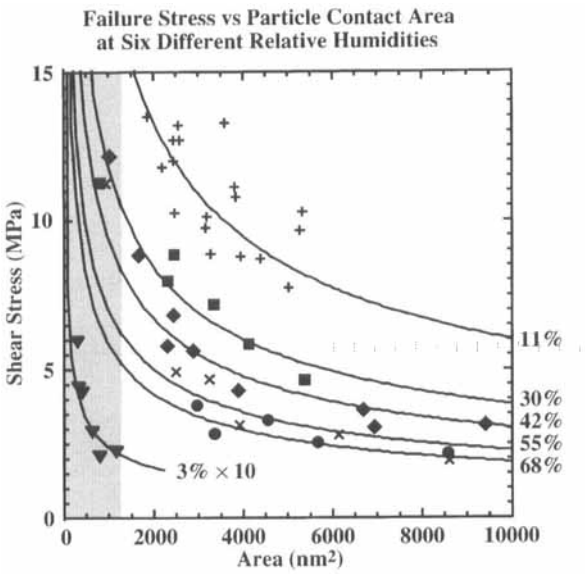

FIGURE 4 Nominal shear stress at failure *vs.* NaCl/glass contact area for NaCl cubes of various sizes at relative humidities ranging from 3% to 68%. Note that the failure stresses at 3% RH have been scaled (reduced) by a factor of ten for convenient display; the smallest particle tested at 3% RH failed at 55 MPa. The dark lines represent one-parameter, least-squares fits to the data, assuming that the nominal shear stress is proportional to $A^{-0.5}$, where A is the area of the NaCl cube in contact with the glass. The shaded region of the graph marks the size range in which the cubes are smaller than the radius of curvature of the SFM tip.

raising the humidity dramatically decreases σ_c. Particle size (here parameterized by the contact area, A) also strongly affects the shear strength, especially for the smaller particles. Both effects impose experimental limits on the size of particles amenable to study at the lowest humidities, where the SFM tip may break before a large particle will be removed. This is consistent with anecdotal reports of the difficulty of particle removal from surfaces under dry conditions. Significantly, increasing the humidity beyond 50% has little additional effect on the shear stress at failure. Similarly, the particle-size dependence becomes weak for particles with contact areas larger than 3000 – 4000 nm^2.

The effect of humidity on shear strength is quantified in Figure 5, where the failure stress for particles with nearly equal contact areas (5000 nm^2) is plotted as a function of relative humidity. (The value for 3% RH has been extrapolated due to our inability to remove

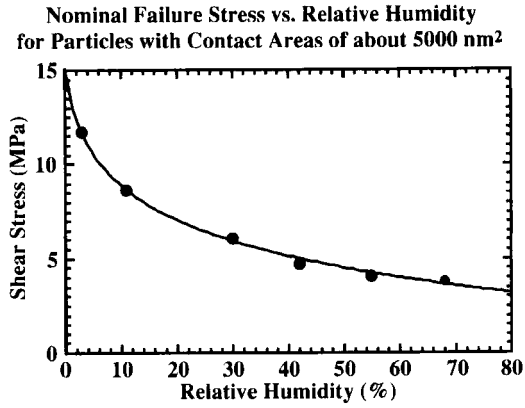

FIGURE 5 A plot of the peak lateral forces observed for cubes of nominal contact area 5000 nm^2 ($\sim 70\,nm \times 70\,nm$) as a function of relative humidity. The point for the lowest RH (= 3%) is extrapolated from the data, due to the difficulty of removing particles of this size at RH = 3%.

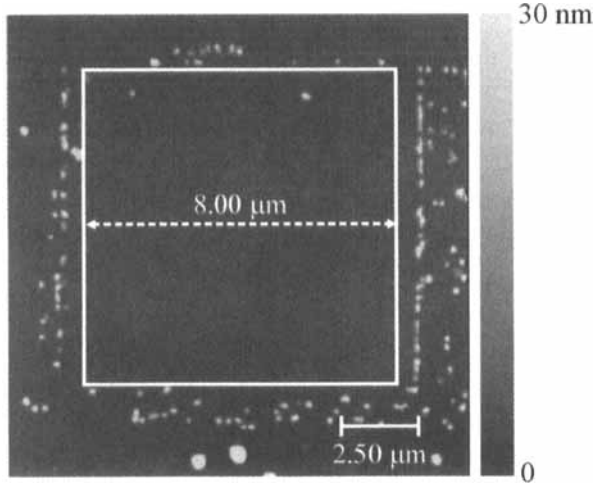

FIGURE 6 A SFM image of a region of the substrate cleared of adhering NaCl particles at 55% RH and a contact force of 51 nN.

particles of this size at low RH.) The failure stress drops rapidly with increasing RH in the lower humidity range, and falls more gradually at the higher humidities. The dark line represents a least squares fit of a model to the data, described below.

At high RH, relatively large particles can be removed from the substrate at modest contact forces. Under these conditions, the SFM tip can be used to remove virtually all the particles from large areas. The results of such a sweeping procedure at 55% RH and 51 nN contact force are shown in Figure 6. An $8 \times 8\,\mu m^2$ area has been swept clean of NaCl particles, and the resulting debris is piled up around the edges, exhibiting a fair amount of order due to their alignment. This illustrates the effectiveness of *combined* chemical and mechanical stimuli in particle manipulation.

4. DISCUSSION

4.1. Chemically-assisted Crack Growth

Considerable effort has been devoted to the understanding of chemically-assisted crack growth, often designated environmental crack growth. Nevertheless, a universal, detailed understanding of it has not yet been achieved. For the purposes of discussion, we adopt a description outlined by Lawn [2] who treats crack growth as a stress-activated chemical reaction. This picture grew out of studies by Wiederhorn, Michalske, Freiman, Bunker, and Lawn. (See Ref. [2] and references therein.) In this approach, the crack velocity, V, is represented as the product of a classical "attempt frequency", f_0 (a typical vibrational frequency), a "crack propagation distance per successful attempt", a_0 (a typical intermolecular spacing), and a probability factor equal to the fraction of attempts yielding a broken bond. Ignoring the reverse reaction (crack healing), classical kinetic theory yields:

$$V = a_0 f_0 \exp(-\Delta F/\mathrm{k}T) \tag{1}$$

where k is Boltzmann constant, T is the temperature, and ΔF is the free energy change associated with fracture in a chemically-active environment.

The effect of chemical environment and stress on ΔF is conveniently described in terms of the relevant energy terms. The chemical environment affects the energy per unit area required to form new fracture surfaces, R. Classically, increasing the stress increases the

available elastic strain energy per unit area to drive crack growth, G (the strain energy release rate). In classical fracture (Griffith) theory, crack growth occurs when $G > R$. An alternate approach, adopted here, is to replace G with the appropriate stress intensity factor, K, where $K=(G\mathrm{E})^{1/2}$ and E is the relevant Young's modulus. K reflects the magnitude of the stress singularity at the tip of an infinitely sharp crack. Replacing G with K is not a trivial change; in chemical terms the difference corresponds roughly to the difference between a stress-activated process (with G) and a volume-activated process (with K). We adopt the stress intensity description because it provides a more consistent description of our data. In general, the question of which description is to be preferred in chemically-assisted crack growth has not been settled. In previous studies of stress-enhanced dissolution of atomic steps on single crystal surfaces, a similar comparison of stress- *vs.* volume-activated mechanisms also favored a volume-activated process [17, 18].

In our case, it is convenient to express the effect of stress on crack velocity in terms of the excess available mechanical energy (proportional to K) over the energy required to form the fracture surfaces (proportional to R). Expanding ΔF in terms of this difference yields

$$\Delta F = \Delta F_0 + (\alpha K - \beta R) + \cdots \tag{2}$$

where $\Delta F_0 = \Delta F$ when $\alpha K = \beta R'$, and α and β are constants of proportionality. Equation (1) then becomes

$$V = a_0 f_0 \exp(-\Delta F_0/\mathrm{k}T) \exp[(\alpha K - \beta R)/\mathrm{k}T] \tag{3}$$

In this formalism, the effect of mechanical stress and chemical attack on crack growth reduces to finding appropriate expressions for K and R. Although we do not measure the crack velocity *per se*, the exponential dependence of crack velocity on K and R assures that velocities which yield fracture on a given experimental time scale will be associated with similar values of $(K - R)$. In the limit of low crack speeds (typically $< 10\,\mu\mathrm{m/s}$), R is a simple function of RH. At sufficiently high crack speeds, R becomes less dependent on humidity due to the inability of diffusing vapor to keep up with the advancing crack tip. The strong effect of humidity in this work indicates that the time-to-failure is dominated by crack growth in the low velocity limit. In all

cases, failure on a given experimental time scale requires that the crack velocity [and, thus, $(K - R)$] be large enough to produce failure while the tip is applying a significant lateral force to the particle. We treat the minimum K value for failure on a given time scale (here determined by the tip velocity) as a critical value for failure and denote it as K_c. In general, raising the humidity will lower R and, thus, lower K_c.

The applied stress intensity, K, is a function of sample geometry, including crack geometry, and is generally treated numerically. For a cube bound to a planar substrate with a small, sharp interfacial crack, K is expected to scale as

$$K \sim a\sigma_{xy} c^{1/2} \tag{4}$$

where σ_{xy} is the nominal shear stress applied to the particle (lateral force divided by particle/substrate contact area), c is the crack length, and a is a constant of order 3 [19]. A complication in our loading scheme is the effect of the normal (compressive) stress exerted by the SFM tip on the adhering particles. This compressive stress tends to close any existing crack and effectively reduces K. For the purpose of analysis, we assume this effect is independent of particle size. (Proportionally higher compressive stresses are expected for particles shorter than the radius of curvature of the SFM tip. The shaded region in Figure 4 identifies data points where this may be a factor.) Assuming that all particles of a given size have (at least statistically) similar interfacial flaws, we can replace K_c with σ_c, where $\sigma_c = \sigma_{xy}$ at detachment.

In Figure 4 we presented these critical values of shear stress as a function of the nominal particle/substrate contact area, A, for several values of relative humidity. The monotonically decreasing shear stress with area led us first to a two-parameter curve fit of $\sigma_c \sim A^{-n}$ for each value of RH. Each fit yielded $n = 0.5$ to within the uncertainty of the curve-fitting procedure (typically ± 0.1). The dark lines in the figure represent one-parameter least-squares fits of a function proportional to $A^{-1/2}$. This dependence is quite reasonable if we assume that the size of the initial interfacial flaws at the perimeter of the particles scale with particle area. [Assuming failure occurs at $K = K_c$ in Eq. (4), constant for a given RH, $\sigma_{xy} \sim K_c\, c^{-1/2} \sim A^{-1/2}$ requires that c is proportional to A.] This model suggests that flaw size is responsible for the area dependence of the failure stress.

Humidity influences σ_c through its effect on R. Raising the partial pressure of water vapor lowers R, which in turn lowers K_c and σ_c. For interfacial failure,

$$R = \gamma_{glass} + \gamma_{salt} - \gamma_{salt-glass} - \Delta U_{glass} - \Delta U_{salt}, \quad (5)$$

where γ_{glass} and γ_{salt} are the two surface energies after detachment ($\gamma_{glass} \neq \gamma_{salt}$), $\gamma_{salt-glass}$ is the interfacial energy before detachment, and ΔU_{glass} and ΔU_{salt} are the *changes* in the two surface energies due to the reactions with water vapor.

The adsorption energy is a complex function of humidity and surface coverage, especially at high relative humidities where more than one monolayer of water may cover the surface. For submonolayer coverages, the Langmuir isotherm describes the adsorption in many adsorbate/substrate systems. It also provides a convenient empirical description of adsorption in the present case. For the Langmuir isotherm, $\Delta U = 2\Gamma_m \ln(p/p_0)$ [2], where Γ_m is the adsorption energy per unit area for full (monolayer) coverage, p is the partial pressure of the adsorbate in the surrounding atmosphere (here proportional to the relative humidity), and p_0 is the partial pressure at which the coverage equals half a monolayer. In the present context, full coverage will amount to several monolayers of water on both glass and NaCl, so the interpretation of these values will be somewhat strained. This problem is mitigated somewhat by the hydrophilic nature of glass and salt surfaces, which ensures that water–glass and water–salt bonds are much stronger than water–water bonds. Thus, the total energy of water sorption will be dominated by the energy of the first monolayer. With these assumptions, the crack velocity as a function of σ_{xy} and partial pressure, p, become:

$$V = a_0 f_0 (1 + p/p_0)^{2\alpha\Gamma_m} \exp[-(2\gamma + \Delta F_0)/kT] \exp[\alpha' \sigma c^{1/2}/kT]. \quad (6)$$

Again assuming that interfacial fracture occurs on experimental time scales for cracks that reach a critical speed, σ_c for NaCl cubes of a given contact area will scale as:

$$\sigma_c = m \ln[n/(1 + p/p_0)] \quad (7)$$

where m, n, and p_0 are parameters. A fit of Eq. (7) to experimental data for particles with contact areas close to 5000 nm^2 appears in Figure 5. The model describes the data quite adequately.

The kinetics approach to environmental crack growth (Eq. (6)) predicts that temperature changes alter the crack velocity. We plan to explore the effect of temperature on particle removal in future work.

4.2. Work of Adhesion Estimate

Particle detachment requires that work be done against interfacial forces whose origins are electronic in nature. In many systems, dispersion (van der Waals) forces dominate adhesion between dissimilar materials. However, the highly ionic nature of NaCl suggests that electrostatic forces (*via* image charges) may contribute. An understanding of these effects is necessary if the effect of water and other solvents is to be understood on the molecular level. As a first step in this direction, we have estimated the contribution of electrostatic and dispersion forces to adhesion in the salt–glass system.

The electrostatic contribution to the work of adhesion was estimated by performing a Madelung-like sum of the electrostatic potential energy of an array of plus and minus charges (the NaCl crystal) in the presence of a similar array of reduced strength (image charges in the glass). The NaCl crystal was treated as a lattice of charges of magnitude $\pm e$ (where e is the electron charge) with the rocksalt structure and nearest neighbor distance of 2.82 Å (as in NaCl). The glass was treated as a continuous dielectric positioned parallel to one edge of the NaCl lattice, with the interface arbitrarily positioned one-half the nearest neighbor distance from the nearest NaCl plane. (This choice of interface is analogous to treating the glass as a continuous extension of the NaCl crystal.) The magnitude of the dielectric constant, κ, is a key uncertainty in this estimate, due to the contribution of ionic diffusion (which increases in the low frequency limit). For this work, a typical value of κ for soda lime glass at 100 Hz was used ($\kappa = 8.3$) [1]. Reasonable convergence was obtained with NaCl lattices containing 2000 ion pairs, with a corresponding work of adhesion of 20 mJ/m^2.

The contribution of dispersion forces was estimated by computing an appropriate Hamaker constant and assuming an interfacial separation equal to one nearest-neighbor distance in NaCl. The Hamaker constant for the system was taken as the geometric mean of the Hamaker constants for soda lime glass and NaCl, which, in turn, were estimated from the Clausius-Mosotti equation for the

Hamaker constant in terms of the bandgap and high-frequency dielectric constant [20]. This procedure yielded Hamaker constants of 6.2×10^{-20} J and 3.1×10^{-20} J for the salt and the glass, respectively. The resulting contribution to the interfacial work of adhesion amounts to 15 mJ/m^2.

Our estimate of the total work of adhesion, W_{ads}, is equal to the sum of the electrostatic and dispersion contributions, or 35 mJ/m^2. In the near future, we hope to extend these calculations to include the effect of water vapor.

The work of adhesion is related to the energy per unit area required for crack growth, R, by the relation $W_{ads} = \gamma_{glass} + \gamma_{salt} - \gamma_{salt-glass}$ [20]. Equation (5) then yields $R = W_{ads} - \Delta U_{glass} - \Delta U_{salt}$, with $R = W_{ads}$ in the limit of zero humidity. The area under the lateral force curve at 11% RH provides an upper bound on R and, thus, W_{ads} of 50 mJ/m^2. Our estimate of $W_{ads} \sim 35$ mJ/m^2 lies comfortably below this upper bounds. Our estimate is also well below the experimental fracture surface energies for NaCl (~ 0.3 J/m^2) and soda lime glass (4–5 J/m^2) [1], consistent with failure along the interface. Although the precise nature of the interface is not known, the surface exposed by particle removal was indistinguishable from the surrounding surface within the resolution of the SFM. If failure is not ideally interfacial, the deviation cannot be much more than a monolayer.

5. CONCLUSIONS

The lateral forces required to remove particles from a soda lime glass substrate with the tip of a scanning force microscope are strong functions of particle size and relative humidity. At 3% RH, only the smallest particles could be removed by the SFM tip at any accessible contact force. Increasing the RH to 30% dramatically reduces the stress required for particle removal and promotes the removal of much larger particles. Increasing the relative humidity further yields smaller decreases in the failure stress. Clearly, a *combined* chemical and mechanical attack is most effective for particle removal.

The humidity dependence of the failure stress is well described in terms of the energy required to form the final fracture surfaces, where these surfaces are in equilibrium with a given partial pressure of

water vapor. This reduces the energy and, thus, the stress, required for slow crack growth. Although somewhat empirical, the Langmuir isotherm adequately describes the humidity dependence of the stresses required for particle removal. The small size of these particles is important for clear observation of this effect, due to the large perimeter-to-area ratio of the interface. For these particles, the interaction of water vapor with the perimeter of the interface has a significant effect on the strength of the interface as a whole.

Particle removal is an important factor in a number of technologies, including integrated circuit manufacture and optical component manufacture. An improved understanding of these processes should facilitate intelligent redesign of particle removal processes as new particle removal challenges present themselves.

Acknowledgments

This work was supported by the National Science Foundation Surface and Tribology Program under Grant CMS-98-00230 and a National Science Foundation Instrumentation Grant DMR-9201767. We wish to thank Louis Scudiero, WSU, for his assistance in this work and preliminary SFM studies of the NaCl particles on glass, and John Hutchinson, Harvard University, for helpful discussions on fracture mechanics.

References

[1] Kingery, W. D., Bowen, H. K. and Uhlmann, D. R., *Introduction to Ceramics*, 2nd edn. (John Wiley, New York, 1976), pp. 797.
[2] Lawn, B., *Fracture of Brittle Solids*, 2nd edn. (Cambridge University Press, Cambridge, 1993), pp. 378.
[3] Meyer, E., Luthi, R., Howald, L. and Bammerlin, M., In: *Micro/Nanotribology and its Applications*, Bhusan, B., Ed. (Kluwer Academic, Dordrecht, 1997), pp. 193–215.
[4] Junno, T., Deppert, K., Montelius, L. and Samuelson, L., *Appl. Phys. Lett.* **66**, 3627–3629 (1995).
[5] Lebreton, C. and Wang, Z. Z., *J. Vac. Sci. Technol. B* **14**, 1356–1359 (1996).
[6] Westra, K. L. and Thomson, D. J., *J. Vac. Sci. Technol. B* **12**, 3176–3181 (1994).
[7] Williams, P. M., Shakesheff, K. M., Davies, M. C., Jackson, D. E., Roberts, C. J. and Tendler, S. J. B., *Langmuir* **12**, 3468–3471 (1996).
[8] Villarrubia, J. S., *J. Res. Natl. Inst. Stand. Technol.* **102**, 425–454 (1997).
[9] Hutter, J. L. and Bechhoefer, J., *Rev. Sci. Instrum.* **64**, 1868–1873 (1993).
[10] Drexler, K. E., *Nanosystems: Molecular Machinery, Manufacturing, and Computation* (John Wiley & Sons, 1992), pp. 576.

[11] Walters, D. A., Cleveland, J. P., Thomson, N. H., Hansma, P. K., Wendman, M. A., Gurley, G. and Elings, V., *Rev. Sci. Instrum.* **67**, 3583–3590 (1996).
[12] Neumeister, J. M. and Ducker, W. A., *Rev. Sci. Instrum.* **65**, 2527–2531 (1994).
[13] Labardi, M., Allegrini, M., Salermo, M., Frediani, C. and Ascoli, C., *Appl. Phys. A* **74**, 3–10 (1994).
[14] Bhushan, B., *Tribology and Mechanics of Magnetic Storage Devices*, 2nd edn. (Springer, New York, 1996), pp. 499–540.
[15] Chung, D. H. and Buessem, W. R., In: *Anisotropy in Single-Crystal Refractory Compounds*, Vahldiek, F. W. and Mersol, S. A., Eds. (Plenum, New York, 1968), pp. 217–245.
[16] Bull, S. J., Page, T. F. and Yoffe, E. H., *Philos. Mag. Lett.* **59**, 281–288 (1989).
[17] Park, N.-S., Kim, M.-W., Langford, S. C. and Dickinson, J. T., *J. Appl. Phys.* **80**, 2680–2686 (1996).
[18] Scudiero, L., Langford, S. C. and Dickinson, J. T., *Tribology Lett.* **6**, 41–55 (1999).
[19] Hutchinson, J. W., *Personal communication* (1998).
[20] Adamson, A. W., *Physical Chemistry of Surfaces*, 5th edn. (John Wiley, New York, 1990).